Synthesis of 12-Metal Clusters Based on the $[Mo_6Cl_8]^{4+}$ Core. X-ray Structure of $(PPN)_2[Mo_6Cl^i_8\{(\mu\text{-NC})Mn(CO)_2Cp\}^a_6]$

Dean H. Johnston, Charlotte L. Stern, and Duward F. Shriver*

Department of Chemistry, Northwestern University, Evanston, Illinois 60208-3113

Received May 7, 1993•

Reaction of $(Bu_4N)_2[Mo_6Cl^i_8(CF_3SO_3)^a_6]$ with $[CpMn(CO)_2CN]^-$, $[CpMn(CO)(NO)CN]$, or $[CpRu(PPh_3)_2CN]$ leads to replacement of all six $CF_3SO_3^-$ anions by the organometallic ligands, which are attached through the ambident CN^- ligand. The unusual decrease in $\nu(CN)$ upon complex formation appears to arise from increased M–C back-π-bonding and, in one case where it can be assessed, reduced kinematic coupling. A very strong electronic absorption band for these complexes is attributed to mixing of charge transfer with localized transitions. Crystallographic data for $(PPN)_2[Mo_6Cl^i_8\{(\mu\text{-NC})Mn(CO)_2Cp\}^a_6]$: triclinic space group, $P\bar{1}$ (No. 2), a = 17.803(6) Å, b = 19.082(2) Å, c = 29.787(6) Å, α = 73.45(1)°, β = 85.00(2)°, γ = 72.38(2)°, V = 9245(7) Å^3, Z = 3.

Introduction

The cyanide ligand has been used extensively in the design and synthesis of novel polynuclear complexes because of its ability to act as an ambident bridging ligand. Recently a series of bi- and trinuclear μ-CN complexes have attracted attention owing to properties such as intervalent charge transfer,[1-4] intramolecular energy transfer,[5-8] multielectron transfer,[9,10] and electron transfer between remote redox sites.[11] A well-known example of cyanide-mediated charge transfer is Prussian blue,[12] where the intense color is attributed to the light-induced intervalence charge transfer from Fe^{II} to Fe^{III} centers. Indeed, Prussian blue is often given as the classic example of intervalence (IT) charge transfer in mixed-valence complexes.[13,14] In the cubic structure of Prussian blue,[12] each of the iron(III) centers is complexed by six $[Fe^{II}(CN)_6]^{4-}$ "ligands", in essence forming a polynuclear complex extending in three dimensions.

Electron-rich organometallic cyanide complexes greatly extend the range of cyanide-bridged complexes[15-19] because of the enhanced basicity of the cyanide nitrogen. Braunstein, *et al.*[18] recently prepared a unique Mn_4Pd_4 cluster by the reaction of $[Pd_4(CO)_4(OAc)_4](AcOH)_2$ with $Na[CpMn(CO)_2CN]$. The displacement of the acetate ligands on the Pd_4 cluster by the $[CpMn(CO)_2CN]^-$ ligands generated $[(OC)Pd(\mu\text{-NC})Mn(\eta\text{-}C_5H_4Me)(CO)_2]_4$, a cluster containing both Pd–Pd and Mn–Pd bonds along with bridging cyanide ligands.

In the present research, the cyanide complexes $[CpMn(CO)_2CN]^-$ and $CpRu(PPh_3)CN$ serve as ligands to displace the weakly-held triflate ligands on the $[Mo_6Cl^i_8(CF_3SO_3)^a_6]^{2-}$ cluster.[25] The properties of the resulting 12-metal clusters are investigated and discussed.

Experimental Section

All manipulations were performed under an atmosphere of dry N_2 using standard Schlenk and syringe techniques. The solvents CH_2Cl_2, acetone, CH_3CN, Et_2O, and HMPA (hexamethylphosphoramide) were dried over appropriate drying agents (P_2O_5, 4-Å molecular sieves, CaH_2, sodium/benzophenone, and CaO, respectively) and distilled prior to use. $CpMn(CO)_3$, $RuCl_3{\cdot}xH_2O$, and $NO[PF_6]$ were supplied by Strem Chemicals. $CpMn(CO)_3$ was purified by sublimation, and all other reagents were used as received.

The Bu_4N^+, $BzlMe_3N^+$, and PPN^+ salts of $[CpMn(CO)_2CN]^-$ were prepared by the method described by Fischer and Schneider,[20] $CpRu(PPh_3)_2CN$ was synthesized by the method of Baird and Davies,[21] and the Bu_4N^+, $BzlMe_3N^+$, and PPN^+ salts of $[Mo_6Cl^i_8(CF_3SO_3)^a_6]^{2-}$ were prepared by the methods of Johnston *et al.*[25]

Synthesis of $(Bu_4N)_2[Mo_6Cl^i_8\{(\mu\text{-NC})Mn(CO)_2Cp\}^a_6]$ (1). A 100-mL Schlenk flask was charged with 0.200 g (0.0894 mmol) of $(Bu_4N)_2[Mo_6Cl^i_8(CF_3CO_2)^a_6]$, a second flask was charged with 0.240 g (0.541 mmol) of $(Bu_4N)[CpMn(CO)_2CN]$, and 10 mL of CH_2Cl_2 was added to each with dissolution of the solids. Dropwise addition of the $[CpMn(CO)_2CN]^-$ solution to the molybdenum cluster solution produced a deep red-orange solution, which was reduced to 3 mL under vacuum. Diethyl ether was added until very little color remained in solution. The resulting fine orange microcrystalline powder was isolated by filtration, washed with 2 × 10 mL Et_2O and dried *in vacuo* to yield 0.200 g (88%) of product. This was further purified by recrystallization from CH_2Cl_2/Et_2O. IR (CH_2Cl_2, cm^{-1}): 2028 (ν_{CN}), 1916, 1866 (ν_{CO}). FAB-MS: peak at m/z = 2313 (R = 3.84; m/z = 2304–2324) followed by loss

• Abstract published in *Advance ACS Abstracts*, October 1, 1993.

(1) Bignozzi, C. A.; Roffia, S.; Chiorboli, C.; Davila, J.; Indelli, M. T.; Scandola, F. *Inorg. Chem.* 1989, *28*, 4350–4358.
(2) Bignozzi, C. A.; Argazzi, R.; Schoonover, J. R.; Gordon, K. C.; Dyer, R. B.; Scandola, F. *Inorg. Chem.* **1992**, *31*, 5260–5267.
(3) Pfennig, B. W.; Bocarsly, A. B. *J. Phys. Chem.* **1992**, *96*, 226–233.
(4) Dong, Y.; Hupp, J. T. *Inorg. Chem.* **1992**, *31*, 3322–3324.
(5) Bignozzi, C. A.; Roffia, S.; Scandola, F. *J. Am. Chem. Soc.* **1985**, *107*, 1644–1651.
(6) Bignozzi, C. A.; Paradisi, C.; Roffia, S.; Scandola, F. *Inorg. Chem.* **1988**, *27*, 408–414.
(7) Bignozzi, C. A.; Indelli, M. T.; Scandola, F. *J. Am. Chem. Soc.* **1989**, *111*, 5192–5198.
(8) Kalyanasundaram, K.; Grätzel, M.; Nazeeruddin, M. K. *Inorg. Chem.* **1992**, *31*, 5243–5253.
(9) Zhou, M.; Pfennig, B. W.; Steiger, J.; Van Engen, D.; Bocarsly, A. B. *Inorg. Chem.* **1990**, *29*, 2456–2460.
(10) Pfennig, B. W.; Bocarsly, A. B. *Coord. Chem. Rev.* **1991**, *111*, 91–96.
(11) Vogler, A.; Kunkely, H. *Inorg. Chim. Acta* **1988**, *150*, 1–2.
(12) Buser, H. J.; Schwarzenbach, D.; Petter, W.; Ludi, A. *Inorg. Chem.* **1977**, *16*, 2704–2710.
(13) Hush, N. S. *Prog. Inorg. Chem.* **1967**, *8*, 391.
(14) Creutz, C. *Prog. Inorg. Chem.* **1983**, *30*, 1–73.
(15) Rao, K. M.; Prasad, R.; Agarwala, U. C. *Synth. React. Inorg. Met.-Org. Chem.* **1987**, *17*, 469–477.
(16) Deeming, A. J.; Proud, G. P.; Dawes, H. M.; Hursthouse, M. B. *J. Chem. Soc., Dalton Trans.* **1988**, 2475–2481.
(17) Oswald, B.; Powell, A. K.; Rashwan, F.; Heinze, J.; Vahrenkamp, H. *Chem. Ber.* **1990**, *123*, 243–250.
(18) Braunstein, P.; Oswald, B.; Tiripicchio, A.; Camellini, M. T. *Angew. Chem., Int. Ed. Engl.* **1990**, *29*, 1140–1143.
(19) Prasad, R.; Mishra, L.; Agarwala, U. C. *Indian J. Chem.* **1991**, *30A*, 45–52.
(20) Fischer, E. O.; Schneider, R. J. J. *J. Organomet. Chem.* **1968**, *12*, P27–P30.
(21) Baird, G. J.; Davies, S. G. *J. Organomet. Chem.* **1984**, *262*, 215–221.
(22) Cromer, D. T.; Waber, J. T. In *International Tables for X-ray Cystallography;* The Kynoch Press: Birmingham, England, 1974; Vol. IV, Table 2.2A.
(23) Cromer, D. T. In *International Tables for X-ray Cystallography;* The Kynoch Press: Birmingham, England, 1974; Vol. IV; Table 2.3.1.
(24) Ibers, J. A.; Hamilton, W. C. *Acta Crystallogr.* **1974**, *17*, 781.
(25) Johnston, D. H.; Gaswick, D. C.; Lonergan, M. C.; Stern, C. L.; Shriver, D. F. *Inorg. Chem.* **1992**, *31*, 1869–1873.

0020-1669/93/1332-5170$04.00/0

Table I. Cyanide, Carbonyl, and Nitrosyl Stretching Frequencies for Various (Cyclopentadienyl)metal Complexes[a]

formula	ν_{CN}	ν_{CO}	ν_{NO}
$(Bu_4N)_2[Mo_6Cl^i_8\{(\mu\text{-NC})\text{-}Mn(CO)_2Cp\}^a_6]$	2028	1916, 1866	
$(Bu_4N)[CpMn(CO)_2CN]$	2060	1906, 1830	
$[Mo_6Cl^i_8\{(\mu\text{-NC})Mn(CO)\text{-}(NO)Cp\}^a_6](PF_6)_4$	2124	2059	1813
$CpMn(CO)(NO)(CN)$	2122	2046	1797
$[Mo_6Cl^i_8\{(\mu\text{-NC})Ru(PPh_3)_2\text{-}Cp\}^a_6](CF_3SO_3)_4$	2007		
$CpRu(PPh_3)_2CN$	2072		

[a] All spectra taken in CH_2Cl_2. Values reported in cm^{-1}.

Table II. UV–Visible Spectral Data for Mono- and Polynuclear Complexes[a]

formula	λ_{max}	$10^{-4}\epsilon_{max}$[b]
$(Bu_4N)_2[Mo_6Cl^i_8Cl^a_6]$	313	0.32
$(Bu_4N)_2[Mo_6Cl^i_8(CF_3SO_3)^a_6]$	296	0.33
$(Bu_4N)_2[Mo_6Cl^i_8\{(\mu\text{-NC})Mn(CO)_2Cp\}^a_6]$	402	3.8
$(Bu_4N)[CpMn(CO)_2CN]$	365	0.071
$[Mo_6Cl^i_8\{(\mu\text{-NC})Ru(PPh_3)_2Cp\}^a_6](CF_3SO_3)_4$	331	6.0
$CpRu(PPh_3)_2CN$	330	0.30

[a] All spectra taken in CH_2Cl_2. [b] ϵ_{max} in units of L mol^{-1} cm^{-1}.

of $CpMn(CO)_2$, Cp, 2 × CO, and Mn. Anal. Calcd (found) for $C_{80}H_{102}Cl_8N_8Mn_6Mo_6O_{12}$: C, 37.58 (36.93); H, 4.02 (4.10); N, 4.38 (4.34); Mn, 12.89 (12.52); Mo, 22.52 (21.79). The PPN^+ and $BzlMe_3N^+$ salts were synthesized in a similar manner.

Synthesis of $[Mo_6Cl^i_8\{(\mu\text{-NC})Ru(PPh_3)_2Cp\}^a_6](CF_3SO_3)_4$ (2). To a 100-mL Schlenk flask were added 0.100 g (0.0447 mmol) of $(Bu_4N)_2[Mo_6Cl^i_8(CF_3CO_2)^a_6]$ and 0.200 g (0.279 mmol) of $CpRu(PPh_3)_2CN$. The yellow solids were dissolved in 15 mL of CH_2Cl_2, forming an intensely colored yellow solution, and a product precipitated as a yellow powder upon slow addition of Et_2O. The powder was collected on a fine fritted glass filter and dried *in vacuo*. Total yield: 0.175 g (68%). IR (CH_2Cl_2, cm^{-1}): 2007 (ν_{CN}). Anal. Calcd (found) for $C_{256}H_{210}N_6Cl_8F_{12}Mo_6O_{12}P_{12}Ru_6S_4$: C, 53.42 (51.86); H, 3.68 (3.99); N, 1.46 (1.58); Mo, 10.00 (10.60); Ru, 10.54 (10.75).

Chemical Oxidation of (1) with $NO[PF_6]$. A 100-mL Schlenk flask was loaded with 0.050 g (0.020 mmol) of $(Bu_4N)_2[Mo_6Cl^i_8\{(\mu\text{-NC})Mn(CO)_2Cp\}^a_6]$, and a second, with 0.050 g (0.29 mmol) of $NO[PF_6]$. The cluster was dissolved in 5 mL of CH_3CN, and the $NO[PF_6]$ was dissolved in 10 mL of CH_3CN. The latter solution was added dropwise to the solution of **1** until the intense red-orange color no longer persisted and only a yellow solution remained (approximately 8 mL). IR (CH_2Cl_2, cm^{-1}): 2128 (ν_{CN}), 2058 (ν_{CO}), 1813 (ν_{NO}).

Instrumentation. IR spectra were taken either as solution spectra using 0.1 mm path length solution cells or as Nujol mulls using a Bomem MB-100 FT-IR at a resolution of 2 cm^{-1}. Raman spectra were collected using the 647.1-nm line from a Kr^+ laser scattered 180° off a spinning solid sample. UV–visible spectra were recorded with a Cary 1E UV–visible spectrophotometer. All UV–visible spectra were collected using specially designed cells that excluded air. Liquid secondary ion (FAB) mass spectra were run on a VG-70 SE double-focusing high-resolution mass spectrometer. Cesium iodide was used as the primary ion source, and *m*-nitrobenzyl alcohol was used as the matrix. The primary source current was 1 μA, and 30 kV of ion beam was used to sputter the liquid sample surface. Negative-ion detection was used to collect all of the mass spectral data. Metal and C, H, N analyses were performed by Elbach Analytical Laboratories, Gummersbach, Germany.

X-ray Crystal Structure of $(PPN)_2[Mo_6Cl^i_8\{(\mu\text{-NC})Mn(CO)_2Cp\}^a_6]$. Deep red-orange crystals of $(PPN)_2[Mo_6Cl^i_8\{(\mu\text{-NC})Mn(CO)_2Cp\}^a_6]$ were grown by diffusion of diethyl ether into a CH_2Cl_2 solution of the cluster. A translucent, prismatic crystal of $(PPN)_2[Mo_6Cl^i_8\{(\mu\text{-NC})Mn(CO)_2Cp\}^a_6]$ having approximate dimensions of 0.3 × 0.1 × 0.1 mm was mounted on a glass fiber and transferred to the N_2 cold stream of an Enraf-Nonius CAD-4 diffractometer with graphite monochromated Mo Kα radiation. A set of 25 carefully centered reflections were used to generate a least-squares-refined reduced unit cell corresponding to the triclinic system. The space group (No. 2) was confirmed by the average values of the normalized structure factors and the successful solution and refinement of the structure. The data were collected at a temperature of −120 ■ 1 °C using the ω–θ scan technique to a maximum 2θ value of 46.0°. This gave 26 633 total reflections, 25 652 unique reflections, and 7828 observed ($I > 3.00\sigma(I)$) reflections. A summary of the crystallographic data is given in Table III. The intensities of three standard reflections were monitored every 90 min, and no appreciable decay was observed. The data were corrected for secondary extinction (coefficient = 0.2718×10^{-8}), Lorentz, and polarization effects. Numerical absorption corrections were also applied, resulting in transmission factors ranging from 0.62 to 0.88.

Table III. Crystal Data for $(PPN)_2[Mo_6Cl^i_8\{(\mu\text{-NC})Mn(CO)_2Cp\}^a_6]$

empirical formula	$Mo_9Cl_{12}P_6O_{15}N_{12}C_{180}H_{135}Mn_9$
M_r	4675.31
crystal size, mm	0.3 × 0.1 × 0.1
crystal system	triclinic
space group	$P\bar{1}$ (No. 2)
a, Å	17.803(6)
b, Å	19.082(2)
c, Å	29.787(6)
α, deg	73.45(1)
β, deg	85.00(2)
γ, deg	72.38(2)
V, Å^3	9245(7)
Z	3
ρ(calcd), g cm^{-3}	1.68
μ(Mo Kα), cm^{-1}	14.2
λ, Å	0.710 73
T, °C	−120
$R(F)$[a]	0.073
$R_w(F)$[b]	0.070

[a] $R(F) = \sum||F_o| - |F_c||/\sum F_o$. [b] $R_w(F) = [\sum w(|F_o| - |F_c|)^2/\sum w|F_o|^2]^{1/2}$.

All calculations were performed using the TEXSAN crystallographic software package. The structure was solved by direct methods (SHELXS-86). Neutral-atom scattering factors[22] and anomalous dispersion terms[23,24] were taken from the literature. The unit cell contained 1.5 cluster units with one cluster located on an inversion center. One manganese atom [Mn(8)] and one carbonyl [C(81), O(81)] were found to be disordered over two sites, labeled A and B, and refined to site occupancies of 0.3918 and 0.6082, respectively. The carbonyl atoms, C(81A/B), and O(81A/B), were refined with group isotropic thermal parameters. All metal, chlorine, and phosphorus atoms except one of the disordered manganese atoms (Mn8A) were refined aniosotropically. The cation phenyl rings and the cyclopentadienyl rings on Mn(7) and Mn(8) were refined as idealized rings. All remaining non-hydrogen atoms were refined with isotropic thermal coefficients. Hydrogen atoms were not included in the structure factor calculations. The carbon atom from one of the carbonyls on Mn(7) never surfaced in the final difference map. The final cycle of full-matrix least-squares refinement converged to an R value of 0.073 ($R_w = 0.070$). The maximum and minimum peaks in the final difference Fourier map corresponded to 1.16 and −0.92 e/Å^3, respectively, and were located in the vicinity of the molybdenum atoms. A satisfactory refinement was not obtained in space group $P1$. An ORTEP diagram of the anion of $(PPN)_2[Mo_6Cl^i_8\{(\mu\text{-NC})Mn(CO)_2Cp\}^a_6]$ is shown in Figure 1, and positional parameters for the anion are given in Table IV. Selected distances and angles for the structure of $(PPN)_2[Mo_6Cl^i_8\{(\mu\text{-NC})Mn(CO)_2Cp\}^a_6]$ are given in Table V.

Results and Discussion

The new polynuclear cyanide-bridged compounds $(Bu_4N)_2[Mo_6Cl^i_8\{(\mu\text{-NC})Mn(CO)_2Cp\}^a_6]$ (**1**) and $[Mo_6Cl^i_8\{(\mu\text{-NC})Ru(PPh_3)_2Cp\}^a_6](CF_3SO_3)_4$ (**2**) are readily prepared by the reaction of electron-rich cyanide complexes with the lightly-coordinated Mo(II)–chloride cluster $(Bu_4N)_2[Mo_6Cl^i_8(CF_3SO_3)^a_6]$. Both complexes are soluble in CH_2Cl_2, CH_3CN, HMPA, and acetone, and spectroscopic data indicate the metal–cyanide complex is not displaced from the cluster by these solvents. Complex **1** is mildly air sensitive and slightly light sensitive, whereas **2** appears to be quite stable to light and air both in solution and as a solid.

The structure of $(PPN)_2[Mo_6Cl^i_8\{(\mu\text{-NC})Mn(CO)_2Cp\}^a_6]$, the anion of which is diagramed in Figure 1, consists of a $[Mo_6Cl^i_8]^{4+}$ core coordinated by six $[CpMn(CO)_2CN]^-$ complexes. Crystallographic data for the structure of $(PPN)_2[Mo_6Cl^i_8\{(\mu\text{-NC})Mn(CO)_2Cp\}^a_6]$ are given in Table III, positional parameters are listed in Table IV, and selected bond distances and angles are given in Table V. The molybdenum atoms are numbered Mo-

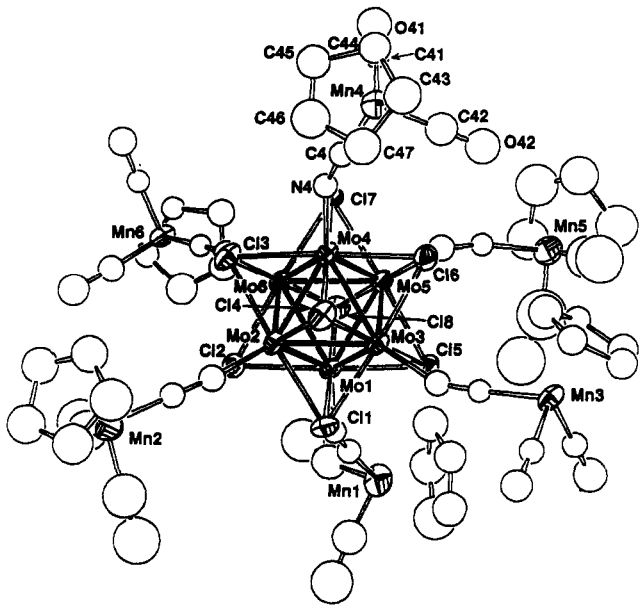

Figure 1. ORTEP diagram of the anion of $(PPN)_2[Mo_6Cl^i_8\{(\mu\text{-}NC)Mn(CO)_2Cp\}^a_6]$. Thermal ellipsoids are drawn at 50% probability. The labeling scheme is outlined in the text.

(1)–Mo(9), and the numbering of the $[CpMn(CO)_2CN]^-$ groups is based on the molybdenum atom to which the group is bound; i.e., the cyanide bound to Mo(1) is labeled N(1) and C(1), then Mn(1), C(11), C(12), etc. The $[Mo_6Cl^i_8]^{4+}$ core is essentially identical to the structures of previously characterized molybdenum halide clusters.[25-30] The average Mo–N bond length is 2.10 Å, the average Mn–C bond length is 1.89 Å, and the average C–N distance is 1.15 Å. The Mo–N–C angles range from 154 to 168°, and the average Mo–N–C angle is 160°. The Mn–C–N angles for the nondisordered manganese atoms range from 172 to 180°, and the average Mn–C–N angle is 176°.

The proposed formulations for complexes **1** and **2** were determined by elemental (including metals) analysis. Further confirmation was obtained for complex **1** from the FAB mass spectrum. The broad parent peak was observed at m/z = 2313, which agrees well with the m/z value of 2314 calculated for the species $(Bu_4N)[Mo_6Cl^i_8\{(\mu\text{-}NC)Mn(CO)_2Cp\}^a_6]^-$. An R factor[25] of 3.84 was determined using the calculated and observed intensities over the range m/z = 2304–2324, and this confirms the identity of the parent fragment. Additional peaks at lower m/z correspond to successive loss from the parent ion of a $CpMn(CO)_2$ fragment, a Cp ligand, two CO ligands, and finally a Mn atom. This fragmentation pattern is interesting, as it indicates the Mn–CN bond is cleaved more readily than the Mo–NC bond. Attempts to obtain positive-ion FAB mass spectra of **2** were unsuccessful, presumably due to its high mass (>5000) and high cationic charge.

The position of the CN stretching frequency in the infrared spectrum and its shift with respect to the unbridged species are shown in Table I. The value of ν_{CN} is lowered from the CN stretch observed for the unbridged complexes by about 30 and 60 cm^{-1} for compounds **1** and **2**, respectively. This shift is opposite from the shift observed for the majority of bridging cyanide complexes, where both electronic and kinematic factors increase ν_{CN} upon bridge formation.[31,32] Bignozzi *et al.*[2] considered a large number of polynuclear cyanide-bridged complexes and their unbridged counterparts, some of which display a red shift as observed for **1** and **2**. They attribute shifts in ν_{CN} to three major factors: (i) kinematic coupling; (ii) back-bonding from metal to cyanide carbon; (iii) back-bonding from metal to cyanide nitrogen. In most cases, kinematic coupling dominates and the overall shift is to higher wavenumber. When there is significant M→C back-bonding, as shown by the low ν_{CN} for both $[CpMn(CO)_2CN]^-$ and $CpRu(PPh_3)_2CN$, electron withdrawal from the nitrogen end of the cyanide is thought to increase the degree of M→C back-bonding and weaken the C–N bond. For example, Christofides *et al.*[33] observed a 12–15-cm^{-1} decrease in ν_{CN} for Mn–CN–Ru dimers when the N-bonded Ru atom was oxidized. Another example is the observed shift for $[CpRu(PPh_3)_2(CN)H](BF_4)$, which shows a decrease of about 40 cm^{-1} from $CpRu(PPh_3)_2CN$. The possibility of a decrease in ν_{CN} owing to metal to ligand back-π-bonding might also be considered, but this appears unlikely because of the low affinity of molybdenum halide clusters for π acceptor ligands.

Another factor, not considered by Bignozzi *et al.*, is the effect of the M″–N–C bond angle on the degree of kinematic coupling. The results of a simple vibrational calculation based on a kinematic model described by Dows and Haim[31] are shown in the graph in Figure 2. A reduction of the M″–N–C bond angle from 180 to 160° (the average Mo–N–C bond angle in **1**) results in a lowering of ν_{CN} of about 5 cm^{-1}, which corresponds to roughly 10% of the observed shifts.

The reaction of **1** with $NO[PF_6]$ was monitored by infrared spectroscopy and was found to result in a very clean CO substitution, generating $[Mo_6Cl^i_8\{(\mu\text{-}NC)Mn(CO)(NO)Cp\}^a_6]^{4+}$, which was identified by characteristic CN, CO, and NO stretching bands. As shown by the three infrared spectra in Figure 3, there is no sign of side products or decomposition. To confirm that the product was not simply a mononuclear complex such as CpMn(CO)(NO)(CN), $[CpMn(CO)_2CN]^-$ was subjected to oxidation by $NO[PF_6]$ under similar conditions. The reaction was not as clean, but the major product had bands in the carbonyl and cyanide stretching regions of the IR spectrum at 2122 cm^{-1} (ν_{CN}), 2046 cm^{-1} (ν_{CO}), and 1797 cm^{-1} (ν_{NO}). These are similar to the bands observed for the cluster oxidation product, but ν_{CO} and ν_{NO} are both approximately 15 cm^{-1} too low. Addition of a small amount of $(Bu_4N)_2[Mo_6Cl^i_8(CF_3SO_3)^a_6]$ to the solution of "CpMn(CO)(NO)(CN)" produced a product with bands in the IR spectrum identical to those observed for the cluster oxidation product.

It is interesting to note the position of ν_{CN} in the CpMn(CO)(NO)(CN) complexes. The formal oxidation of the Mn atom by NO reduces the availability of electron density on the Mn center for π-back-bonding to the CN ligand. This causes ν_{CN} to shift from 2060 cm^{-1} for $[CpMn(CO)_2CN]^-$ to 2122 cm^{-1} for CpMn(CO)(NO)(CN). This reduced back-bonding also affects the shift in ν_{CN} observed upon coordination of the complex to the $[Mo_6Cl^i_8]^{4+}$ cluster. Whereas a shift to lower wavenumber (2030 cm^{-1}) is observed upon coordination of $[CpMn(CO)_2CN]^-$ to the $[Mo_6Cl^i_8]^{4+}$ cluster, little shift in ν_{CN} is observed upon CpMn(CO)(NO)(CN) coordination to the cluster. The CpMn(CO)(NO)(CN) complex is more easily displaced from the $[Mo_6Cl^i_8]^{4+}$

(26) Brosset, C. *Ark. Kemi, Mineral. Geol.* **1945**, *20A* (7), 1–16.
(27) Brosset, C. *Ark. Kemi, Mineral. Geol.* **1946**, *22A* (11), 1–10.
(28) Chisholm, M. H.; Heppert, J. A.; Huffman, J. C. *Polyhedron* **1984**, *3*, 475–478.
(29) Saito, T.; Nishida, M.; Yamagata, T.; Yamagata, Y.; Yamaguchi, Y. *Inorg. Chem.* **1986**, *25*, 1111–1117.
(30) Preetz, W.; Harder, K.; von Schnering, H. G.; Kliche, G.; Peters, K. *J. Alloys Comp.* **1992**, *183*, 413–429.
(31) Dows, D. A.; Haim, A.; Wilmarth, W. K. *J. Inorg. Nucl. Chem.* **1961**, *21*, 33–37.
(32) Alvarez, S.; López, C.; Bermejo, M. J. *Transition Met. Chem. (London)* **1984**, *9*, 123–126.
(33) Christofides, A.; Connelly, N. G.; Lawson, H. J.; Loyns, A. C.; Orpen, A. G.; Simmonds, M. O.; Worth, G. H. *J. Chem. Soc., Dalton Trans.* **1991**, 1595–1601.
(34) Kettle, S. F. A. Personal communication, 1993.
(35) Fenske, R. F. *J. Am. Chem. Soc.* **1967**, *89*, 253–256.
(36) Lever, A. B. P. *Inorganic Electronic Spectroscopy*, 2nd ed.; Elsevier: Amsterdam, The Netherlands, 1984.

Table IV. Positional Parameters and B_{eq} Values for the Anion of $(PPN)_2[Mo_6Cl^i_8\{(\mu\text{-}NC)Mn(CO)_2Cp\}^a_6]$

atom	x	y	z	B_{eq},[a] Å	atom	x	y	z	B_{eq},[a] Å^2
Mo(1)	0.2191(2)	0.1196(1)	0.13613(9)	2.2(2)	C(8)	0.668(2)	0.589(2)	0.363(1)	5.2(8)
Mo(2)	0.2842(2)	0.2299(1)	0.12319(9)	2.3(2)	C(9)	0.524(1)	0.245(1)	0.4731(8)	2.4(6)
Mo(3)	0.1337(2)	0.2617(1)	0.11045(9)	2.2(2)	C(11)	0.252(2)	−0.140(2)	0.065(1)	7(1)
Mo(4)	0.1855(2)	0.2863(1)	0.18225(9)	2.4(2)	C(12)	0.270(2)	−0.186(2)	0.149(1)	7(1)
Mo(5)	0.1201(2)	0.1777(1)	0.19485(9)	2.4(2)	C(13)	0.119(2)	−0.180(2)	0.142(1)	8(1)
Mo(6)	0.2714(2)	0.1437(1)	0.20723(9)	2.2(2)	C(14)	0.100(2)	−0.113(2)	0.160(1)	7(1)
Mo(7)	0.4078(2)	0.5376(1)	0.46640(9)	2.3(2)	C(15)	0.076(2)	−0.061(2)	0.113(1)	5.6(9)
Mo(8)	0.5534(2)	0.5359(1)	0.44699(9)	2.2(2)	C(16)	0.091(2)	−0.081(2)	0.071(1)	7(1)
Mo(9)	0.5191(1)	0.4086(1)	0.48521(8)	1.9(2)	C(17)	0.121(3)	−0.172(3)	0.091(2)	11(1)
Mn(1)	0.1948(3)	−0.1214(3)	0.1112(2)	4.8(4)	C(21)	0.520(2)	0.256(2)	−0.015(2)	9(1)
Mn(2)	0.5265(3)	0.2879(3)	0.0349(2)	5.3(5)	C(22)	0.568(2)	0.189(2)	0.062(1)	8(1)
Mn(3)	−0.1056(3)	0.4154(2)	0.0109(1)	3.0(4)	C(23)	0.627(2)	0.335(2)	0.022(1)	7(1)
Mn(4)	0.0667(3)	0.5351(2)	0.2228(2)	3.4(4)	C(24)	0.560(2)	0.382(2)	−0.011(1)	8(1)
Mn(5)	−0.1283(3)	0.1107(3)	0.2441(2)	6.4(5)	C(25)	0.498(2)	0.405(2)	0.018(1)	8(1)
Mn(6)	0.4586(3)	−0.0747(2)	0.3260(1)	2.7(3)	C(26)	0.523(2)	0.376(2)	0.067(1)	6(1)
Mn(7)	0.1499(4)	0.6881(3)	0.3801(2)	7.3(6)	C(27)	0.599(2)	0.333(2)	0.072(1)	6(1)
Mn(8A)	0.7476(7)	0.5877(7)	0.3163(4)	3.5	C(31)	−0.126(2)	0.345(2)	−0.007(1)	3.1(6)
Mn(8B)	0.7586(6)	0.6254(6)	0.3385(4)	8(1)	C(32)	−0.068(2)	0.448(1)	−0.044(1)	3.0(6)
Mn(9)	0.5030(2)	0.1529(2)	0.4778(1)	2.2(3)	C(33)	−0.215(2)	0.507(2)	0.009(1)	4.5(8)
Cl(1)	0.2316(4)	0.2041(4)	0.0574(2)	2.9(6)	C(34)	−0.151(2)	0.526(2)	0.023(1)	4.0(7)
Cl(2)	0.3608(4)	0.0950(4)	0.1482(2)	2.9(6)	C(35)	−0.119(2)	0.470(2)	0.067(1)	5.5(8)
Cl(3)	0.3293(4)	0.2503(4)	0.1930(2)	3.3(6)	C(36)	−0.161(2)	0.413(2)	0.078(1)	3.4(7)
Cl(4)	0.1981(4)	0.3623(4)	0.1017(3)	3.3(6)	C(37)	−0.219(2)	0.438(2)	0.044(1)	4.5(8)
Cl(5)	0.0748(4)	0.1554(4)	0.1253(2)	2.9(6)	C(41)	0.057(2)	0.495(1)	0.281(1)	3.0(6)
Cl(6)	0.0433(4)	0.3138(4)	0.1684(3)	3.3(6)	C(42)	−0.017(2)	0.518(2)	0.208(1)	5.0(8)
Cl(7)	0.1731(4)	0.2013(4)	0.2609(2)	3.1(6)	C(43)	0.021(2)	0.653(2)	0.186(1)	6(1)
Cl(8)	0.2035(4)	0.0439(4)	0.2169(2)	3.3(6)	C(44)	0.048(2)	0.648(2)	0.229(1)	4.4(7)
Cl(9)	0.3803(4)	0.4155(4)	0.5043(3)	3.3(6)	C(45)	0.136(2)	0.608(2)	0.232(1)	5.2(8)
Cl(10)	0.6560(4)	0.4128(4)	0.4679(2)	2.9(6)	C(46)	0.154(2)	0.591(2)	0.190(1)	7(1)
Cl(11)	0.5551(5)	0.3441(4)	0.5682(2)	3.6(6)	C(47)	0.088(2)	0.615(2)	0.158(1)	6(1)
Cl(12)	0.4806(4)	0.4838(4)	0.4041(2)	3.0(6)	C(51)	−0.187(3)	0.202(3)	0.206(2)	10(1)
O(11)	0.289(2)	−0.146(2)	0.027(1)	9.9(8)	C(52)	−0.102(3)	0.079(3)	0.196(2)	14(2)
O(12)	0.308(2)	−0.223(2)	0.181(1)	11(1)	C(53)	−0.194(2)	0.129(2)	0.307(1)	8(1)
O(21)	0.514(2)	0.238(2)	−0.048(1)	11(1)	C(54)	−0.238(3)	0.102(2)	0.270(1)	10(1)
O(22)	0.587(2)	0.128(2)	0.089(1)	10.7(9)	C(55)	−0.181(3)	0.025(2)	0.265(1)	10(1)
O(31)	−0.139(1)	0.294(1)	−0.0173(7)	5.7(6)	C(56)	−0.098(3)	0.002(2)	0.293(1)	10(1)
O(32)	−0.040(1)	0.472(1)	−0.0800(7)	4.7(5)	C(57)	−0.127(3)	0.082(3)	0.316(2)	10(1)
O(41)	0.056(1)	0.461(1)	0.3220(8)	5.9(6)	C(61)	0.477(2)	−0.024(1)	0.360(1)	2.8(6)
O(42)	−0.070(1)	0.502(1)	0.1985(7)	5.9(6)	C(62)	0.541(2)	−0.067(2)	0.293(1)	3.8(7)
O(51)	−0.205(2)	0.267(2)	0.182(1)	12(1)	C(63)	0.503(2)	−0.197(2)	0.351(1)	3.5(7)
O(52)	−0.059(2)	0.051(2)	0.163(1)	13(1)	C(64)	0.454(2)	−0.177(2)	0.311(1)	5.8(9)
O(61)	0.488(1)	0.011(1)	0.3845(7)	4.5(5)	C(65)	0.382(2)	−0.140(2)	0.319(1)	4.4(8)
O(62)	0.601(1)	−0.062(1)	0.2714(7)	5.6(5)	C(66)	0.372(2)	−0.126(2)	0.366(1)	4.2(7)
O(71)	0.116(2)	0.597(2)	0.351(1)	12(1)	C(67)	0.449(2)	−0.167(1)	0.385(1)	3.0(6)
O(72)	0.068(2)	0.659(2)	0.466(1)	16(1)	C(72)	0.097(3)	0.669(2)	0.432(2)	9(1)
O(81A)	0.702(4)	0.525(4)	0.251(2)	8(1)	C(73)	0.192(3)	0.782(2)	0.365(2)	22(1)
O(81B)	0.716(3)	0.753(2)	0.392(1)	8.0	C(74)	0.199(3)	0.760(3)	0.324(2)	22(1)
O(82)	0.658(1)	0.738(1)	0.2608(9)	8.0(7)	C(75)	0.124(4)	0.760(3)	0.313(1)	22(1)
O(91)	0.598(1)	0.116(1)	0.3968(6)	4.2(5)	C(76)	0.071(2)	0.783(3)	0.347(2)	22(1)
O(92)	0.639(1)	0.059(1)	0.5363(6)	3.7(4)	C(77)	0.113(3)	0.797(3)	0.380(1)	22(1)
N(1)	0.235(1)	0.023(1)	0.1113(7)	2.9(5)	C(81A)	0.720(6)	0.548(6)	0.275(3)	8(2)
N(2)	0.374(1)	0.266(1)	0.0811(8)	3.4(5)	C(81B)	0.735(4)	0.719(4)	0.377(2)	8.0
N(3)	0.054(1)	0.326(1)	0.0545(7)	3.2(5)	C(82)	0.698(2)	0.685(2)	0.287(1)	6(1)
N(4)	0.165(1)	0.384(1)	0.2078(7)	2.9(5)	C(83)	0.835(2)	0.500(2)	0.357(1)	14.4(9)
N(5)	0.028(1)	0.152(1)	0.2334(8)	3.6(6)	C(84)	0.844(2)	0.531(2)	0.309(1)	14.4(9)
N(6)	0.351(1)	0.067(1)	0.2604(7)	3.0(5)	C(85)	0.863(2)	0.599(2)	0.303(1)	14.4(9)
N(7)	0.302(2)	0.585(1)	0.4269(9)	5.1(7)	C(86)	0.865(2)	0.611(2)	0.347(2)	14.4(9)
N(8)	0.617(1)	0.573(1)	0.3872(8)	3.9(6)	C(87)	0.847(2)	0.550(3)	0.381(1)	14.4(9)
N(9)	0.538(1)	0.302(1)	0.4704(7)	2.9(5)	C(91)	0.560(1)	0.134(1)	0.4304(9)	2.3(6)
C(1)	0.223(2)	−0.034(2)	0.111(1)	3.1(7)	C(92)	0.582(2)	0.098(2)	0.512(1)	4.0(7)
C(2)	0.432(2)	0.275(1)	0.064(1)	3.0(6)	C(93)	0.410(2)	0.149(2)	0.531(1)	3.7(7)
C(3)	−0.004(2)	0.358(1)	0.0363(9)	2.5(6)	C(94)	0.384(2)	0.216(2)	0.492(1)	3.7(7)
C(4)	0.131(2)	0.442(2)	0.214(1)	3.0(6)	C(95)	0.384(2)	0.193(1)	0.450(1)	2.9(6)
C(5)	−0.032(2)	0.136(1)	0.2409(9)	2.7(6)	C(96)	0.414(1)	0.109(1)	0.4632(9)	2.6(6)
C(6)	0.393(1)	0.014(1)	0.2859(9)	2.4(6)	C(97)	0.428(2)	0.083(1)	0.511(1)	2.8(6)
C(7)	0.259(2)	0.622(2)	0.408(1)	6(1)					

[a] $B_{eq} = (8\pi^2/3)\sum_{j=1}^{3} U_{ij} a_i^* a_j^* \vec{a}_i \vec{a}_j$.

cluster than $[CpMn(CO)_2CN]^-$, presumably because of the reduced basicity of CpMn(CO)(NO)(CN) at the cyanide nitrogen atom.

The UV–visible data for complexes **1** and **2** and their precursors are listed in Table II and shown as overlay plots in Figures 4 and 5. Complexes **1** and **2** display broad, very intense absorptions in the visible or near-UV. It can be seen from Figures 4 and 5 that complexes **1** and **2** absorb much more strongly than either the triflate-substituted cluster or the mononuclear complexes, even when corrected for the presence of six Mn or Ru chromophores per complex. Due to the reducing nature of the $[CpMn(CO)_2CN]^-$ and $CpRu(PPh_3)_2CN$ ligands, the intense absorption probably contains some Mn–cluster or Ru–cluster charge transfer character. However, the charge-transfer description (intervalent

Table V. Selected Bond Distances (Å) and Angles (deg) for $(PPN)_2[Mo_6Cl^i_8\{(\mu\text{-}NC)Mn(CO)_2Cp\}^a_6]$[a]

Bond Distances			
Mo(1)–Mo(2)	2.618(4)	Mo(1)–N(1)	2.11(3)
Mo(1)–Mo(3)	2.601(3)	Mo(2)–N(2)	2.10(2)
Mo(1)–Mo(5)	2.604(4)	Mo(3)–N(3)	2.12(2)
Mo(1)–Mo(6)	2.592(4)	Mo(4)–N(4)	2.12(2)
Mo(2)–Mo(3)	2.599(4)	Mo(5)–N(5)	2.03(2)
Mo(2)–Mo(4)	2.594(4)	Mo(6)–N(6)	2.12(2)
Mo(2)–Mo(6)	2.609(3)	Mo(7)–N(7)	2.12(3)
Mo(3)–Mo(4)	2.613(4)	Mo(8)–N(8)	2.09(2)
Mo(3)–Mo(5)	2.604(3)	Mo(9)–N(9)	2.12(2)
Mo(4)–Mo(5)	2.595(4)	Mn(1)–C(1)	1.88(3)
Mo(4)–Mo(6)	2.611(3)	Mn(2)–C(2)	1.87(3)
Mo(5)–Mo(6)	2.607(4)	Mn(3)–C(3)	1.89(2)
Mo(7)–Mo(8)	2.598(4)	Mn(4)–C(4)	1.87(3)
Mo(7)–Mo(8*)	2.601(3)	Mn(5)–C(5)	1.91(3)
Mo(7)–Mo(9)	2.598(3)	Mn(6)–C(6)	1.88(2)
Mo(7)–Mo(9*)	2.608(4)	Mn(7)–C(7)	1.93(3)
Mo(8)–Mo(9)	2.602(4)	Mn(8A)–C(8)	1.90(3)
Mo(8)–Mo(9*)	2.608(4)	Mn(8B)–C(8)	1.95(4)
Mo(1)–Cl(1)	2.474(7)	Mn(8A)–Mn(8B)	1.17(2)
Mo(1)–Cl(2)	2.461(8)	Mn(9)–C(9)	1.86(3)
Mo(1)–Cl(5)	2.476(8)	N(1)–C(1)	1.17(4)
Mo(1)–Cl(8)	2.471(7)	N(2)–C(2)	1.16(4)
Mo(2)–Cl(1)	2.471(9)	N(3)–C(3)	1.13(3)
Mo(2)–Cl(2)	2.450(7)	N(4)–C(4)	1.15(4)
Mo(2)–Cl(3)	2.463(9)	N(5)–C(5)	1.17(4)
Mo(2)–Cl(4)	2.458(7)	N(6)–C(6)	1.17(3)
Mo(3)–Cl(1)	2.468(7)	N(7)–C(7)	1.08(4)
Mo(3)–Cl(4)	2.462(9)	N(8)–C(8)	1.17(4)
Mo(3)–Cl(5)	2.470(9)	N(9)–C(9)	1.18(4)
Mo(3)–Cl(6)	2.465(8)	Mn(1)–C(11)	1.69(4)
Mo(4)–Cl(3)	2.466(8)	Mn(1)–C(12)	1.75(3)
Mo(4)–Cl(4)	2.457(7)	Mn(2)–C(21)	1.79(5)
Mo(4)–Cl(6)	2.473(8)	Mn(2)–C(22)	1.78(4)
Mo(4)–Cl(7)	2.476(7)	Mn(3)–C(31)	1.72(3)
Mo(5)–Cl(5)	2.475(9)	Mn(3)–C(32)	1.73(3)
Mo(5)–Cl(6)	2.470(7)	Mn(4)–C(41)	1.70(3)
Mo(5)–Cl(7)	2.460(9)	Mn(4)–C(42)	1.74(4)
Mo(5)–Cl(8)	2.465(7)	Mn(5)–C(51)	1.84(4)
Mo(6)–Cl(2)	2.458(8)	Mn(5)–C(52)	1.69(6)
Mo(6)–Cl(3)	2.467(9)	Mn(6)–C(61)	1.69(3)
Mo(6)–Cl(7)	2.484(8)	Mn(6)–C(62)	1.72(3)
Mo(6)–Cl(8)	2.487(9)	Mn(7)–C(72)	1.75(5)
Mo(7)–Cl(10*)	2.456(8)	Mn(8A)–C(81A)	1.8(1)
Mo(7)–Cl(11*)	2.460(8)	Mn(8A)–C(82)	1.80(3)
Mo(7)–Cl(12)	2.458(8)	Mn(8B)–C(81B)	2.30(8)
Mo(7)–Cl(9)	2.458(8)	Mn(8B)–C(82)	1.84(3)
Mo(8)–Cl(10)	2.452(6)	Mn(9)–C(91)	1.72(3)
Mo(8)–Cl(11*)	2.462(7)	Mn(9)–C(92)	1.69(3)
Mo(8)–Cl(12)	2.468(9)		
Mo(8)–Cl(8*)	2.47(1)		
Mo(9)–Cl(10)	2.469(8)		
Mo(9)–Cl(11)	2.470(7)		
Mo(9)–Cl(12)	2.466(7)		
Mo(9)–Cl(9)	2.459(8)		

Angles (deg)			
Mo(1)–N(1)–C(1)	154(2)	Mn(1)–C(1)–N(1)	175(2)
Mo(2)–N(2)–C(2)	168(2)	Mn(2)–C(2)–N(2)	178(3)
Mo(3)–N(3)–C(3)	158(2)	Mn(3)–C(3)–N(3)	174(3)
Mo(4)–N(4)–C(4)	158(2)	Mn(4)–C(4)–N(4)	174(3)
Mo(5)–N(5)–C(5)	157(2)	Mn(5)–C(5)–N(5)	172(2)
Mo(6)–N(6)–C(6)	167(3)	Mn(6)–C(6)–N(6)	177(3)
Mo(7)–N(7)–C(7)	166(3)	Mn(7)–C(7)–N(7)	174(3)
Mo(8)–N(8)–C(8)	161(2)	Mn(8A)–C(8)–N(8)	160(3)
Mo(9)–N(9)–C(9)	155(2)	Mn(8B)–C(8)–N(8)	164(3)
		Mn(9)–C(9)–N(9)	180(2)

[a] An asterisk indicates an atom related by a center of inversion.

charge transfer in the case of complex **1**) does not explain the very large molar absorptivities observed for complexes **1** and **2**. The intensity may be due to coupling between the charge-transfer transitions and $[Mo_6Cl^i_8]^{4+}$ cluster-based transitions which occur around 300 nm for the $[Mo_6Cl^i_8(CF_3SO_3)^a_6]^{2-}$ cluster.[34] This type of coupling, also known as "intensity stealing",[35,36] has been

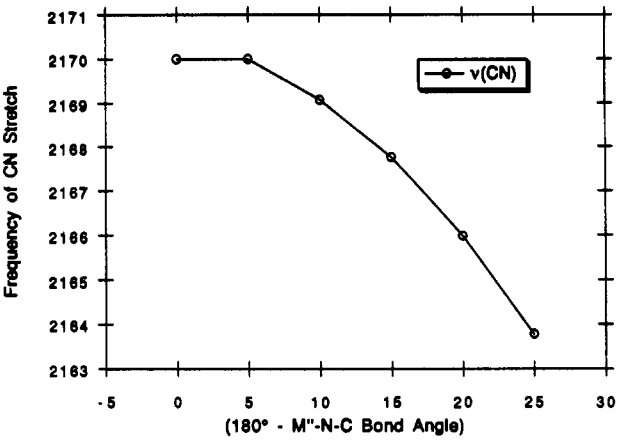

Figure 2. Graph of the C–N stretching frequency (cm^{-1}) calculated as a function of the M''–N–C bond angle in an M''–N–C–M' complex.

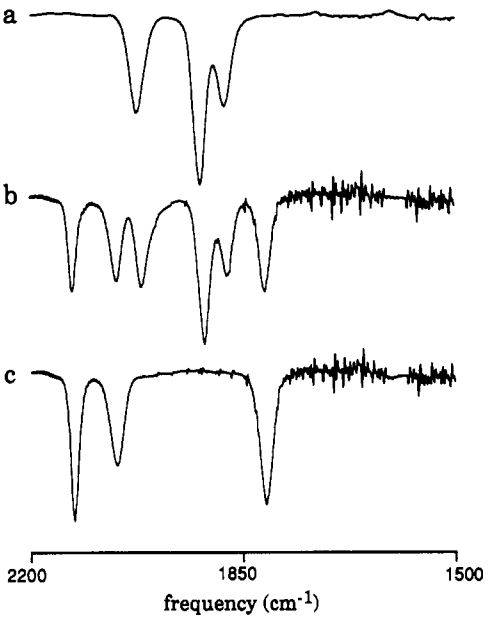

Figure 3. Infrared spectra of $(Bu_4N)_2[Mo_6Cl^i_8\{(\mu\text{-}NC)Mn(CO)_2Cp\}^a_6]$ (**1**) in CH_2Cl_2 (a) prior to oxidation, (b) after ~1 h of stirring with $NO[PF_6]$, and (c) after complete oxidation with $NO[PF_6]$ (~2 h).

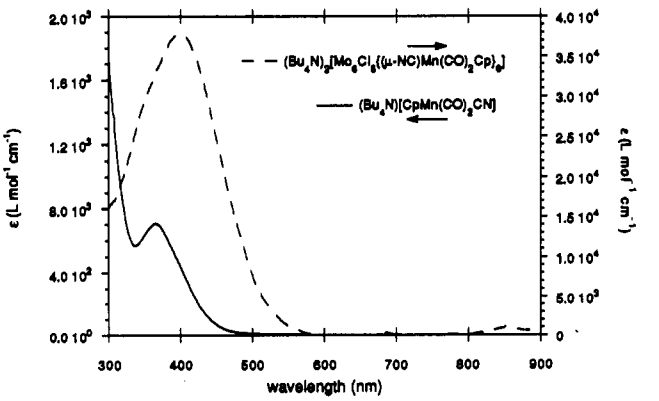

Figure 4. UV–visible spectra (overlay) of $(Bu_4N)[CpMn(CO)_2CN]$ (solid) and $(Bu_4N)_2[Mo_6Cl^i_8\{(\mu\text{-}NC)Mn(CO)_2Cp\}^a_6]$ (**1**) (dashed) taken in CH_2Cl_2. The spectra are plotted on separate scales: $(Bu_4N)[CpMn(CO)_2CN]$ scale on left and $(Bu_4N)_2[Mo_6Cl^i_8\{(\mu\text{-}NC)Mn(CO)_2Cp\}^a_6]$ scale on right.

observed in a number of complexes; examples include the multiply-bonded metal–metal dimers (M = Mo, W, Re, Tc) discussed by Hopkins, Gray, and Misowski,[37] who observed that as the ligands became more reducing, the metal-based $^1(\delta \rightarrow d^*)$ transition both

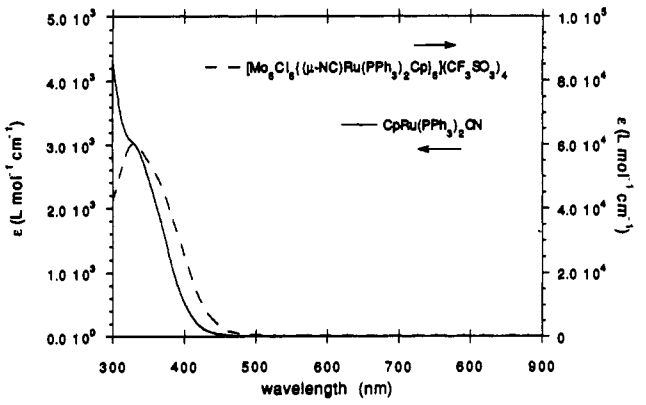

Figure 5. UV–visible spectra (overlay) of $CpRu(PPh_3)_2CN$ (solid) and $[Mo_6Cl^i_8\{(\mu\text{-NC})Ru(PPh_3)_2Cp\}^a_6](CF_3SO_3)_4$ (**2**) dashed) taken in CH_2Cl_2. The spectra are plotted on separate scales: $CpRu(PPh_3)_2CN$ scale on left and $[Mo_6Cl^i_8\{(\mu\text{-NC})Ru(PPh_3)_2Cp\}^a_6](CF_3SO_3)_4$ scale on right.

red-shifted and increased in intensity. The energies and intensities of the electronic absorptions for complexes **1** and **2** fit this trend.

A study of the UV–visible spectrum of complex **1** as a function of solvent polarity revealed a total shift in λ_{max} of 6 nm toward higher energy upon going from CH_2Cl_2 to CH_3CN to HMPA. The shift is very small for a system with charge-transfer transitions, but reduction in solvent sensitivity of charge-transfer bands upon bridge formation has been observed for similar μ-CN bimetallic systems.[8] The direction of the shift (toward higher energy with increasing solvent polarity) agrees with the description of the transition as charge transfer from the Mn center into the cluster.

(37) Hopkins, M. D.; Gray, H. B.; Miskowski, V. M. *Polyhedron* **1987**, *6*, 705–714.

Raman spectra of complex **1** were collected to gain more information about the cluster and specifically about the nature of the visible absorptions. Unfortunately, illumination with intense laser light within the cluster absorption bands caused rapid decomposition with the formation of a black solid. Similar results were obtained with spinning solid samples, spinning solutions, and cooled samples. A Raman spectrum collected with a Kr^+ laser operating at a wavelength well outside the electronic absorption bands, 647.1 nm, has two major low-frequency features at 255 and 310 cm^{-1}, corresponding to Mo–Mo and cluster breathing vibrations of the $[Mo_6Cl^i_8]^{4+}$ core, respectively.[30] Weaker bands observed at 355 and 386 cm^{-1} probably correspond to Mo–N and Mn–C stretching vibrations. Additional Raman scattering was observed at 1858 vw, 1905 s, and 1933 w cm^{-1} (ν_{CO}) and 2029 m and 2041 w cm^{-1} (ν_{CN}). Owing to sample decomposition in the laser beam, attempts to obtain a Raman spectrum of complex **2** were unsuccessful.

Conclusions

The trifluoromethanesulfonate ligands of the lightly-coordinated cluster $(Bu_4N)_2[Mo_6Cl^i_8(CF_3SO_3)^a_6]$ are readily displaced by electron-rich cyanide complexes to form two intensely colored 12-metal clusters: $(Bu_4N)_2[Mo_6Cl^i_8\{(\mu\text{-NC})Mn(CO)_2Cp\}^a_6]$ (**1**) and $[Mo_6Cl^i_8\{(\mu\text{-NC})Ru(PPh_3)_2Cp\}^a_6](CF_3SO_3)_4$ (**2**). The intensities of the visible absorptions of **1** and **2** are due to vibronic coupling between the metal–cyanide charge transfer bands and cluster transitions.

Acknowledgment. This research was sponsored by National Science Foundation Grant No. CHE-9014662.

Supplementary Material Available: Tables of positional parameters, B_{eq} values, thermal parameters, bond distances, and bond angles (24 pages). Ordering information is given on any current masthead page.